# Observed subseasonal variability of oceanic barrier and compensated layers

Hailong Liu, Semyon A. Grodsky, and James A. Carton

*Revision* (2) *for Journal of Climate*
June 8, 2009

Department of Atmospheric and Oceanic Science
University of Maryland, College Park, MD 20742

Corresponding author: Semyon Grodsky (senya@atmos.umd.edu)

**Abstract**

A monthly gridded analysis of barrier layer and compensated layer width based on observed vertical profiles of temperature and salinity and covering the period 1960-2007 is explored for evidence of subseasonal variability and its causes. In the subtropics and midlatitudes this variability is mostly evident during the local cold season when barrier layers and compensated layers are present. There is significant variability of anomalous (non-seasonal) barrier layer and compensated layer width on interannual periods, while in the North Pacific longer term changes are also detectable.

In the winter North Pacific a salinity stratified barrier layer exists at subpolar latitudes. Further south along the Kuroshio extension a compensated layer exists. The width of the barrier layer varies from year to year by up to 60m while compensated layer width varies by half as much. During the observation period the barrier layer width decreased in response to a strengthening of the Aleutian low pressure system, the resulting strengthening of dry northerly winds, and a decrease of precipitation. In contrast, the compensated layer width increased in response to this pressure system strengthening and related amplification of the midlatitude westerly winds, the resulting increase of net surface heat loss, and its effect on the temperature and salinity of the upper ocean water masses.

The tropical Pacific, Atlantic, and Indian Oceans all have permanent barrier layers. Their interannual variability is less than 20m but is comparable in magnitude to the time mean barrier layer width in these areas. In the tropical Pacific west of 160$^{o}$E and in the eastern tropical Indian Ocean, the barrier layer width changes by approximately 5 m in response to a 10 unit change in the South Oscillation Index. It thickens during La Ninas as a result of the presence of abundant rainfall and thins during dry El Ninos. Interannual variations of barrier layer width in the

equatorial Pacific are weak east of 160$^{o}$E with an exception of the area surrounding the eastern edge of the warm pool. Here subduction of salty water contributes to locally stronger variations of barrier layer width.

58 **1. Introduction**

59 The ocean mixed layer is a near-surface layer of fluid with quasi-uniform properties such as
60 temperature, salinity, and density. The width of this mixed layer and its time rate of change both
61 strongly influence the ocean's role in air-sea interaction. However, the width of the near-surface
62 layer of quasi-uniform temperature, MLT, may differ from the width of the near-surface layer of
63 quasi-uniform density, MLD. MLT may be thicker than MLD when positive salinity
64 stratification forms a barrier layer (BL=MLT-MLD) isolating the shallower and deeper levels of
65 the mixed layer as was originally found in the western equatorial Pacific (*Lukas and Lindstrom,*
66 *1991*). Elsewhere MLT may be thinner than MLD when negative salinity stratification
67 compensates for positive temperature stratification (or the reverse situation) to form a
68 Compensated Layer (CL=MLD-MLT) (*Stommel and Fedorov,* 1967*; Weller and Plueddemann,*
69 1996). Changes in the seasonal width of BLs and CLs from one year to the next may cause
70 corresponding changes in the role of the mixed layer in air-sea interaction by altering the
71 effective depth of the mixed layer or the temperature of water at the mixed layer base (e.g., *Ando*
72 *and McPhaden,* 1997). Here we examine the global historical profile observations covering the
73 period 1960-2007 for evidence of corresponding year-to-year changes in the BL and CL width
74 distribution.
75
76 Four studies; *Sprintall* and *Tomczak* (1992), *Tomczak* and *Godfrey* (1994), *de Boyer Montegut et*
77 *al.* (2007), and *Mignot et al.* (2007); have provided an observational description of the seasonal
78 cycle of BL and CL distribution over much of the global ocean. BLs are a persistent feature of
79 the tropics as well as high latitudes during winter. Spatial distribution of BLs in the tropics
80 resembles spatial distribution of the surface freshwater flux. Here BLs occur in regions of high

rainfall and river discharge such as the Arabian Sea and Bay of Bengal, where layers as thick as 20-60m have been observed (*Thadathil* et al., 2008). Similarly, BLs occur in the western Equatorial Pacific under the high precipitation regions of the Intertropical Convergence Zone and South Pacific Convergence Zone (*Lukas and Lindstrom*, 1991; *Ando and McPhaden,* 1997) and in the western tropical Atlantic (*Pailler et al.,* 1999; *Ffield,* 2007).

Impacts of the freshwater forcing on BLs are also evident at high latitudes. Here BLs occur where freshening in the near-surface is produced by excess precipitation over evaporation, river discharge, or ice melting (*de Boyer Montegut et al.*, 2007). In particular, in the Southern Ocean south of the Polar Front BLs occur as a result of near surface freshening due to ice melting and weak thermal stratification (*e.g. de Boyer Montegut et al.*, 2004). BLs produced by the surface freshening may be most evident in regions where upward Ekman pumping ($w_{Ek}$) acts against the effects of vertical mixing such as occurs in the north Pacific subpolar gyre (*Kara et al.,* 2000). In addition to local air-sea interactions, the cross-gyre transport of salty and warm Kuroshio water from the subtropical gyre (that spreads in the subpolar gyre below the fresh mixed layer) contributes to the formation of a stable haline stratification and thus allows a cool mixed layer to exists over a warmer thermocline during winter-spring in the North Pacific subpolar gyre (*Ueno* and *Yasuda,* 2000; *Endoh et al.,* 2004).

At lower latitudes there is a remarkable regularity of BLs appearance equatorward of the subtropical salinity maxima (e.g. *Sato et al.*, 2006). In the subtropical gyres the salinity is high due to permanent excess of evaporation over precipitation and the Ekman downwelling. Here BLs are present due to the subsurface salinity maximum produced by subduction and

104 equatorward propagation of salty water. The subtropical north Pacific provides an example of
105 this. In this region BLs are the result of subduction and southward propagation of salty North
106 Pacific Subtropical Mode Water below fresher tropical surface water (*Sprintall* and *Tomczak*,
107 1992).
108
109 Much less is known about subseasonal variations of BLs and CLs. In their examination of
110 mooring time series *Ando and McPhaden* (1997) show that BLs do have interannual variability
111 in the central and eastern equatorial Pacific and conclude that the major driver is precipitation
112 variability associated with El Nino. At 0$^{o}$N 140$^{o}$W, for example, the BL width increased from
113 10m to 40m in response to the enhanced rains of the 1982-3 El Nino. Precipitation is particularly
114 strong over the western Pacific warm pool. Intense atmospheric deep convection over the high
115 SSTs of the warm pool produces heavy rainfall that promotes formation of thick salt-stratified
116 BLs that, in turn, keep the warm pool SSTs high (*Ando and McPhaden,* 1997). In addition to
117 rainfall, ocean dynamics also contributes to formation of BLs in the western equatorial Pacific.
118 At the seasonal time scales *Mignot et al.* (2007) suggest that changes in zonal advection in
119 response to seasonally varying winds and wind-driven convergence are important in regulating
120 BLs at the eastern edge of the western Pacific warm pool. Recent observations of *Maes et al.*
121 (2006) indicate a close relationship between the longitude of the eastern edge of the warm pool,
122 high SSTs, and the presence of barrier layers. During ENSO cycles the eastern edge of the warm
123 pool shifts in the zonal direction that produces related interannual changes of BLs. In the west
124 observational studies by *Cronin and McPhaden* (2002) and *Maes et al.* (2006) document the
125 response of the mixed layer to intense westerly wind bursts, their fetch, and accompanying
126 precipitation and show how these lead to both the formation and erosion of BLs.

CLs in contrast may result from excess evaporation over precipitation, such as occurs in the subtropical gyres, or by differential advection where it leads to cooler fresher surface water overlying warmer saltier subsurface water (*Yeager* and *Large*, 2007; *Laurian et al.,* 2008). *de Boyer Montegut et al.* (2004) summarize several additional possible mechanisms of CL formation, such as subduction-induced advection, Ekman transport, slantwise convection and density adjustment. CLs are most prominent in the eastern subpolar North Atlantic and in the Southern Ocean (*de Boyer Montegut et al.*, 2007). In the eastern North Atlantic a CL is formed by transport of the warm and salty North Atlantic Current above fresher colder subpolar water. Further east the North Atlantic Current splits into a northern branch comprising the Norwegian and Irminger Currents, and the southward Canary Current, all of which also develop CLs.

Climatological impacts of BLs and CLs have not been comprehensively understood yet. Although the ocean salinity does not have a direct impact on air-sea interactions or SST, the salinity stratification can feed back indirectly to the atmosphere through its influence on the upper ocean density stratification (*Ando and McPhaden,* 1997; *Maes et al.,* 2006; *Ffield,* 2007). In particular *Maes et al.* (2006) suggest that the presence of a BL suppresses heat exchange between the mixed layer and the thermocline by reducing or cutting off entrainment cooling and trapping the heat and momentum fluxes in a shallow surface layer. Thus, a positive feedback between barrier layer formation and warm SSTs is possible. This positive feedback can ultimately lead to formation of SST hot spots (SST>29.75C) observed at the eastern edge of the Pacific warm pool (*Waliser*, 1996). *Foltz* and *McPhaden* (2009) have found that erroneous BLs can bias SST simulations due to improper representation of heat exchange across the bottom of

150 the mixed layer. Much less is known about potential feedbacks of CLs on SST and the
151 atmosphere. Arguably, density compensation within CLs enhances heat exchanges across the
152 bottom of the mixed layer, and thus should provide a negative feedback on SST.
153
154 In this study we build on previous observational examinations of the seasonal cycle of BL and
155 CL development to explore year-to-year variability. This study is made possible by the extensive
156 7.9 million hydrographic profile data set contained in the World Ocean Database 2005 (*Boyer et*
157 *al.*, 2006) supplemented by an additional 0.4 million profiles collected as part of the Argo
158 observing program. We focus our attention primarily on the Northern Hemisphere because of its
159 higher concentration of historical observations.
160
161 **2. Data and methods**
162 This study is based on the combined set of temperature and salinity vertical profiles archived in
163 the World Ocean Database 2005 (WOD05) for the period 1960-2004 and Argo floats from 1997
164 to 2007. Data quality control and processing are detailed in *Carton et al.* (2008) who used the
165 WOD05 profile inventory to explore subseasonal variability of global ocean mixed layer depth.
166
167 Mixed layer depth is defined here following *Carton et al.* (2008) (which in turn combines the
168 approaches of *Kara et al.,* 2000 and *de Boyer Montegut et al.,* 2004) as the depth at which the
169 change in temperature or density from its value at the reference depth of 10m exceeds a specified
170 value (for temperature: $|\delta T| = 0.2^0 C$). This reference depth is sufficiently deep to avoid aliasing
171 by the diurnal signal, but shallow enough to give a reasonable approximation of monthly SST.
172 Because the definition of mixed layer depth is based on the 10m reference depth, our

examination misses features like shallow freshwater lenses (just after intense rainfalls) and other transient processes in the very upper 10m column. The value of $|\delta T| = 0.2^0 C$ is chosen following *de Boyer Montegut et al.* (2004) as a compromise between the need to account for the accuracy of mixed layer depth retrievals and the need to avoid sensitivity of the results to measurement error. The absolute temperature difference instead of the negative temperature difference is used following *Kara et al.* (2000) in order to accommodate for temperature inversions that are widespread at high latitudes[1]. The specified change in density used to define the density-based mixed layer depth follows the variable density criterion (*e.g. Sprintall* and *Tomczak*, 1992) to be locally compatible with the specified temperature value, (i.e. $\delta\rho = (\partial\rho / \partial T) \times 0.2^0 C$ ). In this study the width (or thickness) of either a barrier layer or compensated layer is defined as a difference of isothermal mixed layer depth and isopycnal mixed layer depth, MLT-MLD. The difference MLT-MLD is referred as BL/CL width in this paper. As a result of these definitions a positive MLT-MLD difference (BL/CL width > 0) indicates the presence of a BL while a negative MLT-MLD difference (BL/CL width < 0) indicates the presence of a CL. We compute BL/CL width for each profile. This data are then passed through a subjective quality control to eliminate outliers and averaged into $2^o \times 2^o \times 1$ month grid without any attempt to fill in empty bins.

The total number of binned MLT observations on a $2^o \times 2^o$ monthly grid during 1960-2007 is 1,021,580. Many of these observations are obtained from temperature only profiles measured by either expendable or mechanical bathythermographs; there are only 364,228 (or ~35%) binned

[1] For an example for the vertical profile shown in Fig. 1b of *deBoyer Monte´gut et al.* (2007) our criterion places the MLT at the top of the warm temperature inversion layer while the *deBoyer Monte´gut et al.* (2007) criterion includes the entire subsurface warm layer into the isothermal mixed layer.

194 MLD observations. As expected, the spatial coverage of both MLT and MLD is weighted
195 towards the Northern Hemisphere. North of 10°S there are 271,157 MLD and 788,204 binned
196 MLT observations (~75% of the global total). In this study we use only those vertical casts where
197 both $T$ and $S$ are available, consequently numbers of MLT and MLD observations in this data
198 subset are equal. This study focuses on the cold season variability in each hemisphere. Because
199 the peak of mixed layer deepening lags the midmonth of calendar winter by around one month,
200 we choose January-March (JFM) and July-September (JAS) averages to characterize conditions
201 during northern and southern winter, respectively.
202
203 We explore the role that surface forcing plays in regulating mixed layer properties through
204 comparison of the BL/CL distribution to fluxes from the NCEP-NCAR reanalysis of *Kalnay et*
205 *al.* (1996). Satellite QuikSCAT scatterometer winds (see *Liu,* 2002), which begin in mid-1999,
206 are used to characterize the finer scale spatial patterns of $w_{Ek}$. To better characterize precipitation
207 in the tropics, we also examine the Climate Prediction Center Merged Analysis of Precipitation
208 (CMAP) of *Xie* and *Arkin (*1997), which covers the period 1979 -present.
209
210 In order to quantify the relative impact of temperature and salinity stratification within BLs and
211 CLs we use a bulk Turner Angle, defined following *Ruddick* (1983) as:
212 $Tu_b = \tan^{-1}[(\alpha\Delta T - \beta\Delta S)/(\alpha\Delta T + \beta\Delta S)]$, where $\alpha = \rho^{-1}\partial\rho/\partial T$ (negative) and $\beta = \rho^{-1}\partial\rho/\partial S$
213 (positive) are the expansion coefficients due to temperature, $T$, and salinity, $S$. For negative $\alpha$
214 our definition of $Tu_b$ is consistent with *Yeager and Large* (2007). In this study the changes in
215 temperature and salinity $\Delta T$ and $\Delta S$ are computed between the top, $z_t = \min(MLT, MLD)$, and

the bottom, $z_b = \max(MLT, MLD)$, of either a BL or CL based on analysis of individual vertical profiles. The bulk Turner angle is then evaluated from spatially binned values of $\Delta T$ and $\Delta S$.

There are correspondences between the BL/CL width and the Turner angle. They are illustrated in Table 1 using idealized vertical $T$ and $S$ profiles that includes a perfectly homogeneous mixed layer of depth $H_0$ (isothermal or isopycnal whichever is shallower) with a thermocline and halocline beneath where temperature and salinity vary linearly with depth ($z$).

| **CL** | BL | | | | **CL** |
|---|---|---|---|---|---|
| Bulk Turner angle | | | | | |
| -90° $\tan^{-1}(-3)$ | $\tan^{-1}(-3)$ - 45° | -45° | -45° 45° | 45° | 45° 90° |
| Vertical T-(solid) and S-(dashed) profiles | | | | | |
| 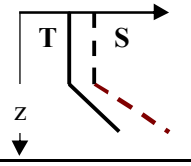 | 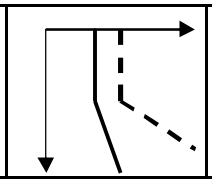 | 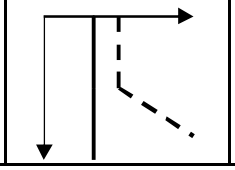 | 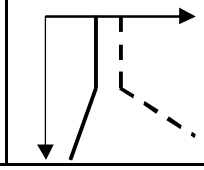 | 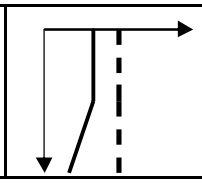 | 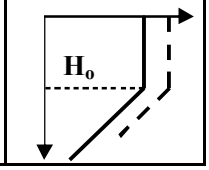 |



Table 1. Bulk Turner angle and idealized vertical profiles of temperature and salinity corresponding to CL and BL. $T_z = \partial T / \partial z < 0$ implies stable stratification ($z$-axis is downward). $H_0$ is isothermal or isohaline layer depth whichever is shallower.

If the top of thermocline is above the top of halocline, the vertical stratification just below $z = H_0$ is similar to the freshwater case ($\partial S / \partial z = S_z = 0$), so that BL=0 and $Tu_b = 45^{\circ}$. In contrast, if the top of halocline is above the top of thermocline, the vertical thermal stratification just below $z = H_0$ is absent ($\partial T / \partial z = T_z = 0$), the BL width could vary significantly while $Tu_b = -45^0$. If for a vertical cast the top of halocline is at the same depth ($z = H_0$) as the top of thermocline, the mixed layer depth based on temperature and density criteria is expressed via corresponding difference criteria ($|\delta T| = 0.2^{\circ}\mathrm{C}$, $\delta\rho = -\alpha|\delta T|$) and vertical gradients,

MLT= $H_0 + |\delta T|/|T_z|$, MLD= $H_0 + \delta\rho / \rho_z$. Switch between the CL and BL regimes occurs when BL=MLT-MLD= $|\delta T|/|T_z| - \delta\rho / \rho_z$ is zero. Noting that $\rho_z = \alpha T_z + \beta S_z$, two solutions of BL=0 exist depending on the sign of $T_z$. If thermal stratification is stable ( $T_z < 0$ ), BL=0 if salinity is homogeneous in the vertical ( $S_z$ =0) and $Tu_b = 45^o$. If thermal stratification is unstable ( $T_z > 0$ ), BL=0 if $2\alpha T_z + \beta S_z = 0$ and $Tu_b = \tan^{-1}(-3) \approx$ -72$^o$.

As seen from the above analysis, the BL width is not a unique function of the Turner angle. For a given $\delta T$ it also depends on $\delta\rho$ (which is a function of $T$ and $S$ ) and on the vertical gradients. In addition, the mixed layer is only approximately homogenous, a fact that contributes to scatter of mixed layer depth (and BL/CL width) estimates especially in situations with weak stratification. Nevertheless, analysis of observed vertical profiles shows a distinct correspondence between values of $\Delta T$ , $\Delta S$ , $Tu_b$ , and the presence of BLs and CLs (**Fig. 1**). Angles $|Tu_b|$<45$^o$ correspond to BLs stabilized by both temperature and salinity ( $\Delta T > 0$ , $\Delta S$ <0). A BL stabilized by salinity but homogeneous in $T$ corresponds to $Tu_b$ =-45$^o$, while $Tu_b$ =45$^o$ corresponds to pure thermal stratification. Angles greater than 45$^o$ correspond to the most frequently occurring CLs where positive temperature stratification compensates for negative salinity stratification (the mixed layer is saltier than the thermocline). Less frequently occurring CLs below cool and fresh mixed layers (-90$^o$< $Tu_b$ < -72$^o$) are observed at high latitudes. The transition point of -72$^0$ is associated with the density ratio $R_\rho = -\alpha\Delta T / \beta\Delta S = 0.5$ or $Tu_b = \tan^{-1}(-3) \approx -72^0$ . For the majority of observed vertical profiles the bulk Turner angle varies between -45$^0$ and 90$^0$. In this range of $Tu_b$ the BL/CL width varies monotonically (to

256 within the scatter of data) as a function of $Tu_b$ (**Fig. 1**). Thus bulk Turner angle in this range
257 provides an alternative way of displaying BL/CL distribution.
258
259 **3. Results**
260 *3.1. Time mean and seasonal patterns*
261 Global seasonal patterns of BL and CL display many features revealed by previous analyses *(de*
262 *Boyer Montegut et al*., 2007). Throughout the year there are persistent BLs in the tropics in areas
263 of high precipitation (**Figs. 2a, 2b**) where our estimates of BL width are similar to previous
264 analysis. In particular, BLs are thick under the Intertropical Convergence Zone and the South
265 Pacific Convergence Zone. BLs are generally thickest on the western side of the tropical Pacific
266 and Atlantic Oceans reflecting higher levels of rain as well as (in the case of the Atlantic)
267 Amazon river discharge. In both the western tropical Pacific and Atlantic Oceans salt advection
268 contributes to the seasonal variation of salinity and BLs (*Foltz et al.,* 2004; *Mignot et al.,* 2007).
269 In contrast to the tropical Pacific and Atlantic (where BLs are thickest in the west) BLs are
270 thickest on the eastern side of the tropical Indian Ocean due to the presence of the Java and
271 Sumatra high precipitation area and freshwater transport from the Bay of Bengal (*Qu* and
272 *Meyers,* 2005). Rainfall in the southern Intertropical Convergence Zone in the South Atlantic
273 (*Grodsky* and *Carton*, 2003) may contribute to freshening of the mixed layer along $10^{o}$S during
274 austral winter. In midlatitudes BL/CLs occur in each Hemisphere mainly during local winter and
275 early spring. In boreal winter BLs exceeding 60 m are observed in the North Pacific subpolar
276 gyre (**Fig. 2a**). Similarly thick BLs occur in the Atlantic Ocean north of the Gulf Stream. In both
277 locations the BLs appear coincident with a seasonal cooling of SST, weakening of thermal
278 stratification, and deepening of MLT. In the north Pacific and the Labrador Sea our estimates of

279 BL width are smaller than BL width by *de Boyer Montegut et al.* (2007). This difference is due to
280 the difference in the definition of temperature-based mixed layer depth. As it is noted above, the
281 *de Boyer Montegut et al.* (2007) MLT estimates are generally deeper in areas of subsurface
282 temperature inversions due to inclusion of the entire depth range of temperature inversion into
283 the mixed layer.
284
285 Sea surface salinity (SSS) increases drastically moving from the cold sector to the warm sector
286 across the Gulf Stream front leading to a switch from the BL regime north of the front to a CL
287 regime south of the front (**Fig. 2a**). Thick CLs (thicker than 30m) are also observed along the
288 Gulf Stream due to cross-frontal transport of low salinity water. And even thicker CLs (thicker
289 than 60m) are observed further northeast along the path of the North Atlantic Current where its
290 warm, salty water overlies cooler, fresher water.[1] Interestingly, despite the presence of warm and
291 salty western boundary currents in both the Atlantic and Pacific Oceans, the winter CLs are much
292 less pronounced in the North Pacific than the North Atlantic. Explanation for this basin-to-basin
293 difference likely lies in the higher surface salinity of the Atlantic (**Fig. 2a**) and consequently
294 larger values of $\Delta S$ (**Fig. 3a**).
295
296 CLs are evident in the southern subtropical gyres of the Pacific and Atlantic Oceans as well as
297 the South Indian and Southwest Pacific Oceans (**Fig. 2b**) south of the 30$^{o}$S SSS maximum. The
298 presence of CLs in these regions reflects the northward advection of cold and fresh water which
299 subducts (due to the downward Ekman pumping) under the water of the SSS maximum
300 (*Sprintall* and *Tomczak*, 1993; *Laurian et al.,* 2008). Note correspondence between CL in **Fig. 2b**

[1] CLs in the North Atlantic and Southern Ocean are not displayed in Fig. 3 of *de Boyer Montégut et al.* (2007) because these CLs have a width which is less than 10% of MLD according to their analysis.

and $\Delta S$ in **Fig. 3b**. A similar subduction mechanism may explain BL formation in subtropical gyres (*e.g. Sato et al.,* 2006). In particular, in the southern Indian Ocean north of 30$^{o}$S BLs form as a result of subduction of salty water from the region of the SSS maximum and the northward propagation of this salty water under relatively fresh surface water (**Fig. 2b**).

The subduction mechanism suggests the BL presence equatorward of the subtropical SSS maximum (where mixed layer tops saltier water below) and the CL presence poleward of the subtropical SSS maximum (where mixed layer is saltier than thermocline). This is evident in a dipole-like meridional pattern of CL and BL in the southern Indian Ocean and adjusted part of the Southern Ocean encompassing the area of SSS maximum along 30$^{o}$S. Similar meridional dipole-like patterns with CLs to the south and BLs to the north of local subtropical SSS maxima are seen during austral winter in the South Pacific and the South Atlantic in the regions of downward $w_{Ek}$ (**Fig. 2b**).

This also appears to hold in the subtropics of the Northern Hemisphere (**Fig. 2a**). In the north Atlantic CLs are observed north of the subtropical SSS maximum (as expected from the subduction mechanism). But, in boreal winter the maximum width CLs in the North Atlantic are observed well north of the downward $w_{Ek}$ regions (**Fig. 2a**). Here CLs extend along the Gulf Stream path and its northern extensions. This, in turn, suggests that in the North Atlantic the horizontal transport of warm salt waters by the western boundary current (rather than the subduction mechanism) contributes to regional CL formation.

Both BLs and CLs accompanying the subtropical maximum of SSS are strongly seasonal (**Fig. 2**) in spite of the permanent presence of subtropical SSS maximum and the Ekman downwelling maintained by trade winds. *Mignot et al.* (2007) have suggested that these permanent factors form background haline stratification while the seasonal variability of BLs is explained by the seasonal deepening of the local MLT during the cold season due to intense wind stirring and negative buoyancy forcing and the presence of a shallow capping halocline. In fact, equatorward of the SSS maximum the subsurface salinity is relatively high because of the presence of salty Subtropical Underwater subducted in the region of the SSS maximum while the surface salinity is relatively low due to the poleward wind-driven advection of fresh equatorial waters (*Foltz et al.,* 2004). In the CL sector the same seasonal deepening of the mixed layer explains the seasonal widening of CLs. Here the injection of saltier mixed layer water into a fresher thermocline ('spice injection' mechanism of *Yeager* and *Large*, 2007) results in stronger density compensation and the widening of CLs during local winter (**Fig. 2**)

Spatial patterns of BL/CL width (**Fig. 2)** are in close correspondence with the spatial patterns of the vertical changes of salinity, $\Delta S$ , (**Figs. 3a, 3b**). As expected, the BLs are distinguished by a stable salinity stratification, $\Delta S < 0$ , where salinity increases downward below the mixed layer. In contrast, CLs have unstable salinity stratification, $\Delta S > 0$ . As discussed above, regions of fresh mixed layer trace major areas of precipitation (like the Intertropical Convergence Zone) and river runoff (the Bay of Bengal). A different type of BL is observed on the equatorward flanks of the subtropical SSS maxima. In these areas the ocean accumulates salt due to an excess of evaporation over precipitation. As discussed in the previous paragraph, here the equatorward propagation of subducted water produces meridional dipole-like BL/CL and $\Delta S$ structures that

346 are most pronounced in the Southern Hemisphere during austral winter (**Figs. 2b, 3b**).

347

348 The spatial patterns of the bulk Turner angle (**Figs. 3e**, **3f**) indicate that the majority of CL cases
349 are associated with warm, salty mixed layer water overlaying colder, fresher water beneath (thus
350 $Tu_b$ >45$^o$). Much rarer CLs can also be formed when cold, fresh water overlays warmer, saltier
351 water ( $Tu_b$ <-72$^o$). This latter type of density compensation is observed only in limited regions of
352 the Labrador Sea during northern winter and near Antarctica during austral winter. The most
353 commonly observed CLs associated with warm and saltier mixed layers ( $Tu_b$ >45$^o$) increase in
354 width during the cold season. This seasonal widening of CL width is attributed by *Yeager* and
355 *Large* (2007) to the seasonal increase in $Tu_b$ that is produced by the spice injection and results in
356 stronger density compensation, thus thicker CLs. The similarity of **Figs. 3e, 3f** to Figure 7 of
357 *Yeager* and *Large* (2007) where $Tu_b$ is computed in the upper 200-m column indicates that
358 during the cold season the vertical changes of temperature and salinity within the BL/CL depth
359 range have the same sign and roughly the same magnitude as the vertical changes across the
360 upper 200 m water column. But, in the tropical Pacific and Atlantic (where the mixed layer is
361 rather shallow) the *Yeager* and *Large* (2007) analysis shows significant areas of $Tu_b$ >45$^o$. In
362 contrast, our analysis in **Fig. 3** indicates that CLs don't occur in these tropical areas. In these
363 tropical areas $Tu_b$ >45$^o$ in the *Yeager* and *Large* (2007) analysis reflects density compensation
364 due to stable thermal stratification and unstable haline stratification below the Equatorial
365 Undercurrent core where both $T$ and $S$ decrease downward.

366

367 *3.2 Subseasonal variability*

Interannual and longer (subseasonal) variability of BL/CL width is similar in amplitude to seasonal variability (compare **Fig. 4** and **Fig. 2**). In the subtropics and midlatitudes this variability occurs in winter-spring of each Hemisphere when BL/CLs are present. During the rest of the year when subtropical and midlatitudes mixed layers warm and shoal the BL/CLs collapse, so that BL/CL width variability is weak. In the tropics BL/CLs are always present and so is their variability. In particular, the variability of BLs in the western tropical Pacific is ~50% (or more) of the time-mean BL width, which is 10m to 40m in this region (**Figs. 2 and 4**). This BL variability reflects interannual variations of rainfall and currents due to ENSO (*Ando and McPhaden*, 1997). In the western equatorial Atlantic as well the BLs are quasi-permanent due to Amazonian discharge and ITCZ rainfall (*Pailler et al*., 1999; *Foltz et al*., 2004). Interannual variability of BLs in this region is comparable in width to the time-mean BL width, which is 5m to 20m. This interannual variability is produced by interannual variation of river discharge as well as by anomalous meridional shifts of the Atlantic ITCZ. Time mean BLs vanish and their subseasonal variability is weak in the eastern tropical Atlantic and Pacific and along the eastern subtropical coasts of the Atlantic and Pacific (**Fig. 4**), where the mixed layer shoals due to equatorial and coastal upwellings. The zonal distribution of BL width variability is reversed in the tropical Indian Ocean where BLs are thickest and their variability is stronger in the east due to strong rainfall over the maritime continent and surrounding areas as well as freshwater transport from the Bay of Bengal.

Subseasonal variability is stronger at higher latitudes reflecting weaker temperature stratification there. Weaker temperature stratification implies a stronger relative impact of freshwater fluxes and other factors on density stratification. The highest variability of BL/CL width (of up to

100m) occurs in winter in the North Atlantic along the routes of northward propagation of warm and salty Gulf Stream water. In these regions the vertical temperature and salinity stratification is similar to that in the subtropical gyres where CLs are formed as a result of the presence of a warmer and saltier mixed layer above a fresher thermocline. As warm and salty Gulf Stream water propagates northward, the temperature stratification weakens (due to the surface cooling), so that CLs widen.

Spatial patterns of CLs are different in the North Pacific in comparison with the North Atlantic. In contrast to the North Atlantic, the near surface layer is relatively fresh in the North Pacific in response to abundant local rainfall. This surface freshwater forcing produces stable haline stratification. In addition to that the haline stratification is affected by exchanges across the Kuroshio-Oyashio extension front. These exchanges result in the expansion of Kuroshio waters into the subpolar gyre where they form a warm and salty subsurface maximum (*Endoh et al.,* 2004). This stable halocline is further maintained by the surface freshwater flux and the upward Ekman pumping. In winter when the MLT deepens in response to the surface cooling, this stable halocline produces 20m to 60m wide BLs (**Fig. 2a**) with subseasonal variation of similar magnitude (**Fig. 4a**).

Time correlations of anomalous BL/CL width with other mixed layer parameters suggest the mechanisms that govern the subseasonal variability of BL/CL. In **Fig. 5** we focus on the northern winter (JFM) when BL/CL width increases in the Northern Hemisphere. This data allows only qualitative examination because of short time series. During JFM, only ~50000 gridded observations are available globally that translates into an average of 5 observations at each grid

414 point, so only large scale correlation patterns matter. Over much of the global ocean BL/CL
415 width is negatively correlated with the bulk Turner angle (**Fig. 5a**). Most BL cases are associated
416 with fresh mixed layers and stable thermal stratification ($-45^o < Tu_b < 45^o$) while most CL cases are
417 associated with salty mixed layers ($45^o < Tu_b < 90^o$) (**Fig. 3**). In this combined range $-45^o < Tu_b < 90^o$
418 the BL/CL width decreases with increasing $Tu_b$ (**Fig. 1**). In some northern areas including the
419 subpolar Pacific, the cold sector of the Gulf Stream, and the Norwegian Sea BL width is
420 positively correlated with $Tu_b$. All these areas are distinguished by the presence of temperature
421 inversions bottoming fresh BLs (**Figs. 3a, 3c**). These vertical stratifications correspond to -
422 $72^o < Tu_b < -45^o$ where the BL width increases with $Tu_b$ (**Fig. 1**). BL width reaches maximum at
423 $Tu_b = -45^o$ which corresponds to shallow fresh BL inside a deeper homogeneous temperature
424 layer.
425
426 Negative correlations between BL/CL width and MLD are similarly widespread **(Fig. 5b**). For
427 BLs this negative correlation means the shallower the fresh density-based mixed layer is, the
428 wider is the depth range separating the bottom of the MLT and MLD. For CLs that are associated
429 with salty mixed layers, deepening of the density-based mixed layer suggests salt injection into
430 the thermocline leading to stronger density compensation, and wider CLs (*Yeager* and *Large*,
431 2008). In contrast to mostly negative correlation with MLD, BL/CL width tends to be
432 positively/negatively correlated with depth of MLT in barrier layer/compensated layer regions,
433 respectively (**Fig. 5c**). The positive correlation in BL regions is better seen and may be explained
434 using the same arguments as those employed by *Mignot et al.* (2007) to explain the seasonal
435 variability of BLs. A variety of factors (surface freshwater fluxes, fresh water advection, etc.)
436 produce shallow haline stratification. Year-to-year changes in the surface forcing affect the

437 seasonal deepening of the MLT during the cold season. In the presence of a shallow capping
438 halocline, these interannual variations of MLT (which define the base of the BL) explain
439 variations of BL width.
440
441 We next consider BL/CL width separated by season and roughly 15-year averaging periods (**Fig.**
442 **6**). In contrast to significant variability of anomalous BL/CL width on interannual and longer
443 periods (**Fig. 4**), the decadal means are similar during the three averaging periods shown in **Fig.**
444 **6.** This suggests that much of the BL/CL width variability occurs at interannual periods except in
445 the north Pacific where long term changes are also detectable. During the first period 1960-1975
446 thick BLs are evident during local winter in the North Pacific, western tropical Pacific and
447 Atlantic, northern Indian Ocean, and Southern Ocean (the latter being evident even in austral
448 summer). CLs during this early period appear primarily in the eastern North Atlantic. Little can
449 be said about the existence of BLs in the Southern Ocean in austral winter due to the lack of data
450 during this period. By the latest period, 1991-2007 several changes are evident. CLs have
451 appeared in the subtropical North Pacific during winter replacing BLs. Elsewhere in the North
452 Pacific the width of the BLs has shrunk. Vertically wide CLs are also evident on the northern
453 side of the Circumpolar Current during austral winter (in fact these may have existed earlier but
454 simply not been observed). In contrast to the North Pacific the North Atlantic doesn't exhibit
455 similar long term changes (or these changes are not detectable with our dataset[1]) even though the
456 winter-spring meteorology of this region does exhibit decadal variations (*Hurrell*, 1995). The last
457 period averages (1991-2007) are computed twice: including the latest Argo data (**Figs. 6c, 6g**),
458 and based on the original WOD05 profile inventory (**Figs. 6d, 6h**) that doesn't include massive

[1] Our data shows interannual thickening of CLs in the north Atlantic in response to interannual strengthening of the North Atlantic Oscillation (NAO) during the Argo period (1997-2007), but the long term response of CLs to the secular strengthening of the NAO during the second half of the 20-th century doesn't manifest in our data set.

459 Argo float deployments of recent years. The two averages look similar and confirm the presence
460 of long term changes of BL/CL width in the North Pacific. We next examine monthly time series
461 of BL/CL width in the north Pacific focusing on two adjacent regions: (1) BLs in the subpolar
462 North Pacific (NP/BL box) and (2) CLs in the subtropical North Pacific (NP/CL box) outlined in
463 **Fig. 6**.
464
465 *3.3 North Pacific*
466 The monthly time series of the northern subpolar North Pacific BL region and the subtropical CL
467 region both show long-term changes towards thinner BLs and thicker CLs interrupted by
468 occasional interannual reversals **(Figs. 7a, 7b)**. Indeed, the subtropical CL region actually
469 supported a 10-20m thick BL prior to 1980s. One direct cause of this change from BL to CL is
470 the gradual deepening of the late winter-spring mixed layer in the central North Pacific noted by
471 *Polovina et al.* (1995) and *Carton et al.* (2008). This observed 20 m deepening into the cooler,
472 fresher sub-mixed layer water has the effect of strengthening density compensation (the 'spice
473 injection' mechanism is discussed by *Yeager* and *Large*, 2007). *Carton et al.* (2008) attribute the
474 cause of mixed layer deepening to changes in the atmospheric forcing associated with the
475 deepening of the Aleutian sea level pressure low after 1976. These changes led to strengthening
476 of the midlatitude westerlies and the ocean surface heat loss in the North Pacific, hence the
477 deepening of the mixed layer. The deepening of the mixed layer has opposite impacts on the
478 width of CLs and BLs. It widens CLs by injecting saltier water from the mixed layer into fresher
479 thermocline. In contrast, stronger atmospheric forcing and related deepening of the mixed layer
480 normally destroys near-surface BLs by enhancing mixing. These mechanisms likely explain the
481 narrowing of BLs and the widening of CLs in the North Pacific during recent decades (**Figs. 7a,**

482 **7b**).

483

484 Correlation analysis in **Fig. 8** indicates an association of the BL and CL width in the NP/BL and
485 NP/CL boxes both seem to be associated with wind changes resulting from changes in the
486 Aleutian surface pressure low. Widening of CLs in the NP/CL box is linked to anomalously
487 strong westerly winds and a positive latent heat loss anomaly in the box **(Fig. 8a).** These two
488 factors produce anomalous deepening of the mixed layer by amplifying wind stirring and
489 convection. In the NP/CL box, the observed CL width increases in phase with deepening of the
490 mixed layer (see inlay in **Fig. 8a**). This in-phase relationship is in line with the 'spice injection'
491 mechanism of *Yeager* and *Large* (2007). In contrast to vertical widening of CLs in the NP/CL
492 box the BLs in the NP/BL box shrink when the local mixed layer deepens (**Fig. 8a**). Possible
493 reason for this shrinking is the direct impact of wind stirring on BLs (as discussed in previous
494 paragraph). Another reason for this shrinking is changes in the surface freshwater flux itself. In
495 fact, the anomalous wind pattern that produces westerly wind strengthening in the NP/BL box
496 includes also anomalous northerly winds to the west of the Aleutian low. These anomalous
497 northerly winds decrease moisture transport from the south and thus reduce the precipitation in
498 the NP/BL box vital to maintaining the BL (**Fig. 8b**). Anomalously weak rainfall leads to
499 shrinking of BLs in the NP/BL box. Shrinking of BLs occurs in-phase with widening of CLs in
500 the NP/CL box (just as in **Figs. 7a, 7b**).

501

502 Coherent variability of January-March CL width and MLD in the NP/CL box is evident in **Fig.**
503 **9a**. Besides the correspondence on decadal scales, both CL width (that is negative) and MLD
504 display apparent out-of-phase interannual variations, so that widening of CLs occur in-phase

505 with deepening of the mixed layer. Variability of MLD in the box follows the variability of the
506 winter Pacific Decadal Oscillation Index (PDO) of *Mantua et al.* (1997) in line with previous
507 findings of *Deser et al.* (1996) and *Carton et al.* (2008). Although in phase changes of MLD and
508 PDO do not hold during some years between 1980 and 1992, the time correlation between the
509 two variables at zero lag evaluated during the entire period 1960-2007 is ~0.6 and exceeds the
510 99% level of zero correlation that is 0.4 (see also Figure 7 in *Carton et al.* (2008)).
511 Correspondence of the mixed layer variability and the PDO suggests a link to variability of
512 midlatitude westerly winds that, in turn, is linked to variability of the strength of the Aleutian
513 low. In fact, this link is revealed by the time correlation analysis of the entire 1960-2007 records
514 in **Fig. 8a**. Variability during particular interannual events also seems to be related to similar
515 changes in winds. In particular, in winter of 1979 the westerly winds were weak in the southern
516 part of the NP/CL box (**Fig. 9b**). As a result, the mixed layer was relatively shallow (~65m deep,
517 **Fig. 9a**) and CLs were missing and replaced by BLs produced by winter rainfall. By the next
518 winter the westerly winds in the box are amplified due to the expansion of the Aleutian low
519 (compare areas within the 1000 mbar contour in **Figs. 9b** and **9c**) and its southward shift.
520 Enhanced mixing and convection due to stronger winds deepened the mixed layer down to
521 120m, injected saltier mixed layer water into the thermocline, and produced 10m wide CLs (**Fig.**
522 **9a**).
523
524 *3.4 Tropical Oceans*
525 The origin of persistent BLs in the tropics (**Fig. 2**) is ultimately linked to tropical precipitation.
526 Direct correspondence of BL width with local precipitation is observed in the far western
527 equatorial Pacific (*Mignot et al.*, 2007). But in some tropical regions the lateral freshwater

528 transport or three-dimensional circulation may also affect the BL width. In particular, the lateral
529 transport of Amazon discharge water, freshwater transport from high rainfall and river discharge
530 areas along with local precipitation are all important for BL formation in the western tropical
531 Atlantic (*Pailler et al.*, 1999; *Foltz et al.*, 2004; *Mignot et al.*, 2007) as well as in the eastern
532 equatorial Indian Ocean (*Qu* and *Meyers,* 2005). In the western tropical Pacific at the eastern
533 edge of the warm pool (where fresh water of the pool converges with saltier water to the east)
534 BLs are affected by subduction of salty water in the convergence zone (*Lukas* and *Lindstrom*,
535 1991).
536
537 Similar processes are involved at interannual time scales (*Ando and McPhaden,* 1997; *Cronin*
538 *and McPhaden,* 2002). During La Nina when the Southern Oscillation Index is positive (SOI>0)
539 tropical rainfall increases in the far western tropical Pacific and eastern tropical Indian Ocean
540 (90E to 160E) by 1 mm/dy or 20% of the local time mean rainfall (in response to a 10 unit
541 decrease of the SOI) (**Fig. 10b**). This western increase is accompanied by decreased rainfall over
542 the rest of the tropical Pacific while Amazonian and tropical Atlantic rainfall increase. As a
543 result of these changes in rainfall BL width in the western Pacific west of 160$^{o}$E, which is
544 normally 10-20m, increases by 5m (**Figs. 10a, 10c**). Thus, in the far western Pacific and eastern
545 tropical Indian Ocean variations in BL width respond primarily to changes in surface freshwater
546 flux. In the Atlantic sector excess discharge associated with the increases of rainfall over the
547 Amazon doesn't result in an expected widening of BL (**Fig. 10a**). Possibly this lack of response
548 may be because much of the Amazon discharge is transported in the Brazilian coastal zone.
549
550 The BL response to ENSO variability has local peak between the dateline and 170$^{o}$W (**Fig. 10a**).

551 During El Ninos the eastern edge of the Pacific warm pool expands into this zone accompanied
552 by weakening upwelling and an eastward shift in the direction of near-surface currents to
553 eastward (see e.g. Fig.2 in *McPhaden*, 2004). The anomalous wind-driven downwelling creates
554 conditions favorable for developing of BLs at the eastern edge of the warm pool via the *Lukas*
555 and *Lindstrom* (1991) mechanism. Conversely, during La Ninas the warm pool contracts
556 westward while strengthened easterly winds strengthen upwelling that, in turn, reduces (or shuts
557 down) the subduction mechanism. So the negative correlation seen between 180E-190E in **Fig.**
558 **10a** reflects formation of BLs in vicinity of the eastern edge of the warm pool during El Ninos
559 and the absence of these BLs during La Ninas.
560
561 **4. Summary**
562 This study examines subseasonal changes in barrier and compensated layer (BL and CL) width
563 based on analysis of observed profiles of temperature and salinity covering the years 1960-2007.
564 Because of data limitations we focus mainly on the Northern Hemisphere and tropics. The
565 processes that regulate subseasonal variability of BL/CL width are similar to those which
566 regulate their seasonal appearance: fluctuations in surface freshwater flux, Ekman pumping, and
567 processes regulating mixed layer deepening. Thus, the spatial distribution of subseasonal
568 variability reflects aspects of the subseasonal variability of these forcing terms. Companion
569 studies (e.g. *Foltz et al.*, 2004; *Mignot et al.,* 2007) suggest that contribution of lateral freshwater
570 advection is also important.
571
572 In the subtropics and midlatitudes during late winter-spring we find alternating regions of CLs
573 and BLs in the seasonal climatology. The northern tropics of both the Pacific and Atlantic (the

574 southern edge of the subtropical gyres) show broad regions of BLs where salty subtropical
575 surface water formed further north has subducted, advected equatorward, and affected the water
576 properties of the winter mixed layer. Within the evaporative subtropical North Pacific and eastern
577 North Atlantic we find CLs resulting from mixed layers with positive temperature stratification
578 but negative salinity stratification. In the subtropics and midlatitudes variability occurs mostly
579 during the local cold season when BLs and CLs are present. In the winter subpolar North Pacific
580 a salinity stratified BL exists which does not have a counterpart in the North Atlantic, while
581 further south along the Kuroshio extension a CL exists. Much of the BL/CL width variability
582 occurs at interannual periods except in the North Pacific where longer term changes are
583 detectable. The width of this BL varies from year to year by up to 60m at some grid points while
584 CLs to the south experience variations of approximately half that. Longer-term variability results
585 from strengthening of the Aleutian pressure low during successive winters, thus strengthening
586 the midlatitude westerly winds leading to deeper mixed layers, cooler SSTs, and a long-term
587 increase in the width of the CL to the south. The same changes in meteorology which include
588 strengthening of the Aleutian pressure low also lead to an increase in dry northerly winds which
589 in turn cause a thinning of the area average northern BL width from ~40m before 1980s to ~ 20m
590 afterwards.
591
592 In the tropics the origin of persistent BLs is ultimately linked to precipitation. Precipitation in the
593 tropics varies strongly interannually. During high precipitation years the mixed layer in this
594 region shows capping fresh layers and thick BLs. In contrast, during low precipitation years
595 mixed layer salinities increase and BL width decreases. In particular, in the western equatorial
596 Pacific and eastern Indian Ocean between 90$^{o}$E and 160$^{o}$E, the BL (which is normally 10-20m

wide in this area) thickens by 5m during La Nina while during El Nino the BL thins by a similar amount in line with previous analysis of *Ando and McPhaden* (1997). During La Nina rainfalls weaken in the tropical Pacific east of 160E which causes a minor decrease of BL width in the central and eastern tropical Pacific. But the BL width response to ENSO forcing amplifies between the dateline and 170$^{o}$W. This amplification is related to BL formation due to salt water subduction near the eastern edge of the warm pool. This subduction strengthens during El Nino (when local equatorial upwelling is suppressed) and weakens during La Nina (when upwelling is restored).

Determining the basin-scale BL/CL structure tests the limits of the historical observing system. Further progress in understanding BL/CL variability and its role in air-sea interactions will likely require further exploration of models that provide reasonable simulations of observed variability.

**Acknowledgements** We gratefully acknowledge the Ocean Climate Laboratory of the National Oceanographic Data Center/NOAA and the Argo Program upon whose data this work is based. Support for this research has been provided by the National Science Foundation (OCE0351319) and the NASA Ocean Programs. The authors appreciate comments and suggestions given by anonymous reviewers.

615 **References**


616 Ando, K., and M.J. McPhaden, 1997: Variability of surface layer hydrography in the tropical
617 Pacific Ocean. *J. Geophys. Res.*, **102**, 23063-23078.

618 Boyer, T.P., J.I. Antonov, H.E. Garcia, D.R. Johnson, R.A. Locarnini, A.V. Mishonov, M.T.
619 Pitcher, O.K. Baranova, and I.V. Smolyar, 2006: *World Ocean Database 2005.* S. Levitus,
620 Ed., NOAA Atlas NESDIS 60, U.S. Government Printing Office, Washington, D.C., 190 pp.,
621 DVDs.

622 Carton, J.A., S.A. Grodsky, and H. Liu, 2008: Variability of the Oceanic Mixed Layer, 1960–
623 2004. *J. Climate***, 21,** 1029–1047.

624 Cronin, M. F., and M. J. McPhaden, 2002: Barrier layer formation during westerly wind bursts.
625 *J. Geophys. Res.,* **107**(C12), 8020, doi:10.1029/2001JC001171.

626 de Boyer Montégut, C., G. Madec, A. S. Fischer, A. Lazar, and D. Iudicone, 2004: Mixed layer
627 depth over the global ocean: An examination of profile data and a profile-based climatology.
628 *J. Geophys. Res*., **109**, C12003, doi:10.1029/2004JC002378.

629 de Boyer Montégut, C., J. Mignot, A. Lazar, and S. Cravatte, 2007: Control of salinity on the
630 mixed layer depth in the world ocean: 1. General description. *J. Geophys. Res*., **112**, C06011,
631 doi:10.1029/2006JC003953.

632 Deser, C., M.A. Alexander, and M.S. Timlin, 1996: Upper-Ocean Thermal Variations in the
633 North Pacific during 1970–1991. *J. Climate*, **9**, 1840–1855.

634 Endoh T., H. Mitsudera, S.-P. Xie, and B. Qiu, 2004: Thermohaline structure in the subarctic
635 North Pacific in a general circulation model. *J. Phys. Oceanogr.*, **34**, 360–371.

636 Ffield, A., 2007: Amazon and Orinoco River Plumes and NBC Rings: Bystanders or Participants
637 in Hurricane Events? *J. Climate*, **20**, 316–333.

638 Foltz, G.R., S.A. Grodsky, J.A. Carton, and M.J. McPhaden, 2004: Seasonal salt budget of the
639 northwestern tropical Atlantic Ocean along 38°W, *J. Geoph. Res*., **109** (C3), C03052,
640 doi:10.1029/2003JC0021112004.
641 Foltz, G.R., and M.J. McPhaden, 2009: Impact of Barrier Layer Thickness on SST in the Central
642 Tropical North Atlantic. *J. Clim*., **22**, 285-299.
643 Grodsky, S. A., and J. A. Carton, 2003: Intertropical convergence zone in the South Atlantic and
644 the equatorial cold tongue. *J. Climate*, **16**(4), 723-733.
645 Hurrell, J. W., 1995: Decadal trends in the North-Atlantic oscillation - regional temperatures and
646 precipitation. *Science,* **269**, 676-679.
647 Kalnay, E., & co-authors, 1996: The NCEP/NACR 40-year reanalysis project. *Bull. Amer.*
648 *Meteor. Soc*., **77**, 437-471.
649 Kara, A. B., P. A. Rochford, and H. E. Hurlburt, 2000: Mixed layer depth variability and barrier
650 layer formation over the North Pacific Ocean. *J. Geophys. Res*., **105**(C7), 16,783–16,801.
651 Laurian, A., A. Lazar A, G. Reverdin, 2008: Generation mechanism of spiciness anomalies: an
652 OGCM analysis in the North Atlantic subtropical gyre. *J. Phys. Oceanogr*., **39**, 1003–1018,
653 doi:10.1175/2008JPO3896.1.
654 Liu, W.T., 2002: Progress in scatterometer application. *J. Oceanogr.,* **58**(1), 121-136.
655 Lukas, R., and E. Lindstrom, 1991: The mixed layer of the western equatorial Pacific Ocean. *J.*
656 *Geophys. Res*., **96** (Supplement), 3343 –3357.
657 Maes, C., K. Ando, T. Delcroix, W. S. Kessler, M. J. McPhaden, and D. Roemmich, 2006:
658 Observed correlation of surface salinity, temperature and barrier layer at the eastern edge of
659 the western Pacific warm pool, *Geophys. Res. Lett.*, **33**, L06601,
660 doi:10.1029/2005GL024772.

McPhaden, M.J., 2004: Evolution of the 2002/03 El Niño. *Bull. Amer. Meteor. Soc.*, **85**, 677–695.

Mignot, J., C. de Boyer Montégut, A. Lazar, and S. Cravatte, 2007: Control of salinity on the mixed layer depth in the world ocean: 2. Tropical areas. *J. Geophys. Res*., **112**, C10010, doi:10.1029/2006JC003954.

Pailler, K., B. Bourlès, and Y. Gouriou, 1999: The Barrier Layer in the Western Tropical Atlantic Ocean. *Geophys. Res. Lett.,* **26**(14), 2069-2072.

Polovina, J.J., G.T. Mitchum, and G.T. Evans, 1995: Decadal and basin-scale variation in MLD and the impact on biological production in the central and North Pacific, 1960-88. *Deep-Sea Res.,* **42***,* 1701-1716*.*

Qu, T., and G. Meyers, 2005: Seasonal variation of barrier layer in the southeastern tropical Indian Ocean. *J. Geophys. Res*., **110**, C11003, doi:10.1029/2004JC002816.

Ruddick, B., 1983: A practical indicator of the stability of the water column to double-diffusive activity. *Deep-Sea Res.,* **30,** 1105–1107.

Sato, K., T. Suga, and K. Hanawa, 2006: Barrier layer in the North Pacific subtropical gyre. *Geophys. Res Lett*, **31**, L05301, doi:10.1029/2003GL018590.

Sprintall, J., and M. Tomczak, 1992: Evidence of the Barrier Layer in the Surface Layer of the Tropics. *J. Geophys. Res.*, **97**(C5), 7305–7316.

Sprintall, J., and M. Tomczak, 1993: On the formation of central water and thermocline ventilation in the Southern Hemisphere. *Deep Sea Res., Part I,* **40**, 827–848.

Stommel, H., and K. N. Fedorov, 1967: Small-scale structure in temperature and salinity near Timor and Mindanao. *Tellus,* **19***,* 306-325.

682 Thadathil, P., P. Thoppil, R.R. Rao, P.M. Muraleedharan, Y.K. Somayajulu, V.V. Gopalakrishna,
683 R. Murthugudde, G.V. Reddy, and C. Revichandran, 2008: Seasonal Variability of the
684 Observed Barrier Layer in the Arabian Sea. *J. Phys. Oceanogr.*, **38**, 624–638.
685 Tomczak, M., and J. S. Godfrey, 1994: Regional Oceanography: An Introduction, Pergamon
686 Press, New York, 422 pp.
687 Ueno, H., and I. Yasuda, 2000: Distribution and formation of the mesothermal structure
688 (temperature inversions) in the North Pacific subarctic region, *J. Geophys. Res.*, **105**(C7),
689 16885-16897.
690 Waliser, D. E., 1996: Formation and limiting mechanisms for very high sea surface temperature:
691 Linking the dynamics and the thermodynamics, *J. Clim.,* **9**, 161– 188.
692 Weller, R. A., and A. J. Plueddemann, 1996: Observations of the vertical structure of the oceanic
693 boundary layer. *J. Geophys. Res*., **101**, 8789–8806.
694 Xie, P., and P.A. Arkin, 1997: Global Precipitation: A 17-Year Monthly Analysis Based on
695 Gauge Observations, Satellite Estimates, and Numerical Model Outputs. *Bull. Amer. Meteor.*
696 *Soc.*, **78**, 2539–2558.
697 Yeager, S.G., and W.G. Large, 2007: Observational Evidence of Winter Spice Injection. *J. Phys.*
698 *Oceanogr.*, **37**, 2895–2919.

699

| CL | BL | | | | CL |
|---|---|---|---|---|---|
| Bulk Turner angle | | | | | |
| -90° $\tan^{-1}(-3)$ | $\tan^{-1}(-3)$ - 45° | -45° | -45° 45° | 45° | 45° 90° |
| Vertical T-(solid) and S-(dashed) profiles | | | | | |
| 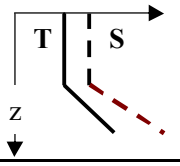  | 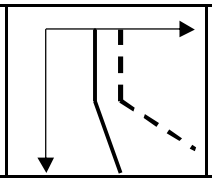 | 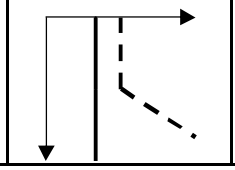 | 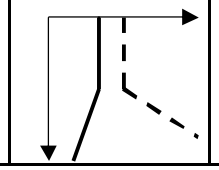 | 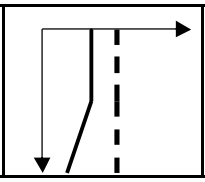 | 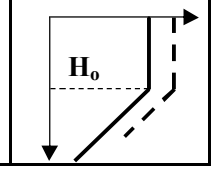  |

700

701 Table 1. Bulk Turner angle and idealized vertical profiles of temperature and salinity

702 corresponding to CL and BL. $T_z = \partial T / \partial z < 0$ implies stable stratification ($z$-axis is downward).

703 $H_0$ is isothermal or isohaline layer depth whichever is shallower.

**Figure captions.**

Figure 1. Observed climatological winter-spring barrier layer/compensated layer width versus bulk Turner angle evaluated using temperature ( $\Delta T$ ) and salinity ( $\Delta S$ ) difference between the top and bottom of a barrier or compensated layer. Vertical bars show the mean and the standard deviation for consecutive $22.5^0$ intervals. Grey dots show January-March data from the Northern Hemisphere and July-September data from the Southern Hemisphere. The Turner angle range - $72^0$ to $45^0$ corresponds to barrier layer. Compensated layer occurs outside this interval.

Figure 2. Observed climatological (a) January-March and (b) July-September barrier layer width (positive) and compensated layer width (negative). Climatological SSS (*Boyer et al.,* 2006, contours), SSS $\geq$ 35 psu (solid), SSS<35 psu (dashed). Areas of downward Ekman pumping are cross-hatched. Ekman pumping is evaluated from the QuikSCAT scatterometer winds of *Liu* (2002).

Figure 3. Observed (a,b) salinity ( $\Delta S$ ) and (c,d) temperature ( $\Delta T$ ) difference between the top $z_t$ = min[MLT, MLD] and bottom $z_b$ =max[MLT, MLD] of barrier/compensated layer, (e,f) bulk Turner angle calculated from $\Delta S$ and $\Delta T$ between the same two depths. (left) January - March (JFM) values, (right) July - September (JAS) values. Turner angles in the range from -$72^o$ to $45^o$ correspond to barrier layers, while compensated layers occur outside this range.

Figure 4. Standard deviation (STD) of observed (a) January-March (JFM) and (b) July-September (JAS) averaged BL/CL width. To contrast variability of barrier layer and compensated layer width, STD deviation is multiplied by the sign of corresponding 3-month

727 average climatological BL/CL width. So the STD of barrier layer/compensated layer width is
728 positive/negative, respectively. All values are computed from 1960-2007 data.
729
730 Figure 5. Time correlation of January-March average (a) BL/CL width and bulk Turner Angle,
731 (b) BL/CL and density based mixed layer depth, (c) BL/CL and temperature based mixed layer
732 depth. N is the total number of JFM average binned observations during 1960-2007. Correlations
733 are shown only at grid points where at least 6 observations are available. Time correlation at
734 every grid point is not significant, only large scale patterns matter.
735
736 Figure 6. Quasi-decadal average barrier layer (positive) and compensated layer (negative) width
737 in (left) northern winter and (right) austral winter. Units are meters. Rectangles show locations of
738 the North Pacific barrier layer box (NP/BL 160$^{o}$E-150$^{o}$W, 45$^{o}$-60$^{o}$N), and the North Pacific
739 compensated layer box (NP/CL 140$^{o}$E-160$^{o}$W, 25$^{o}$-42$^{o}$N). Bottom row shows 1991-2007
740 averages based on the WOD05 data, that doesn't include most of recent Argo data. *N* is the
741 number of 3-month average observations accumulated during each 15 year period over the global
742 ocean. There are a total of 11,000 ocean grid points on a 2$^{o}$x2$^{o}$ grid.
743
744 Figure 7. Box averaged BL/CL width in the (a) North Pacific barrier layer region, (b) North
745 Pacific compensated layer region. Thin lines are 3-month running mean, bold lines are January-
746 March averages. Data are shown if at least 10 measurements are available for box averaging. See
747 Fig.6 for box locations.
748
749 Figure 8. Linear time regression of observed 1960-2007 anomalous JFM BL/CL width in the

North Pacific compensated layer box (see panel a) on anomalous (a) latent heat flux ($Wm^{-2}$/m, shading), 10m winds ($ms^{-1}$/m, arrows), mean sea level pressure (mbar/m, contours) and (b) surface precipitation rate (mm $h^{-1}$/m) elsewhere. BL/CL width time series is inverted, so that regressions correspond to widening of CLs and shrinking of BLs. Areas where time correlation with latent heat flux and precipitation is significant at the 95% level are 'X'-hatched while similar areas for air pressure are '/'-hatched. Inlay shows lagged correlation of anomalous inverted BL/CL width and MLD averaged over (solid) the NP/CL box and (dashed) the NP/BL box. The two box locations are shown in a) and b), respectively. Dashed line is the 95% confidence level of zero correlation. Positive correlation at zero lag implies that CL thickens and BL thins when the mixed layer deepens. Atmospheric parameters are provided by the NCEP/NCAR reanalysis of *Kalnay et al.* (1996).

Figure 9. (a) Times series of JFM BL/CL width and MLD averaged over the NP/CL box, and the PDO index. Data is shown for years with at least 10 measurements available for box averaging. JFM winds and mean sea level pressure (mbar) for years of (b) thin and (c) thick compensated layer. Atmospheric parameters are provided by the NCEP/NCAR reanalysis of *Kalnay et al.* (1996).

Figure 10. Lag regression of SOI on $5^oS$-$5^oN$ averaged (a) anomalous barrier layer width, (b) precipitation (*Xie and Arkin,* 1997). Lag regressions show magnitude in response to 1 unit change of SOI. Solid lines in (a) and (b) are time mean BL width and precipitation. Longitude bands corresponding to land are shaded gray in (a). (c) Time series of annual running mean SOI (shaded) and anomalous BL width averaged over $130^oE$-$160^oE$, $5^oS$-$5^oN$. Data are shown if more

773 that 10 measurements are available for area averaging.

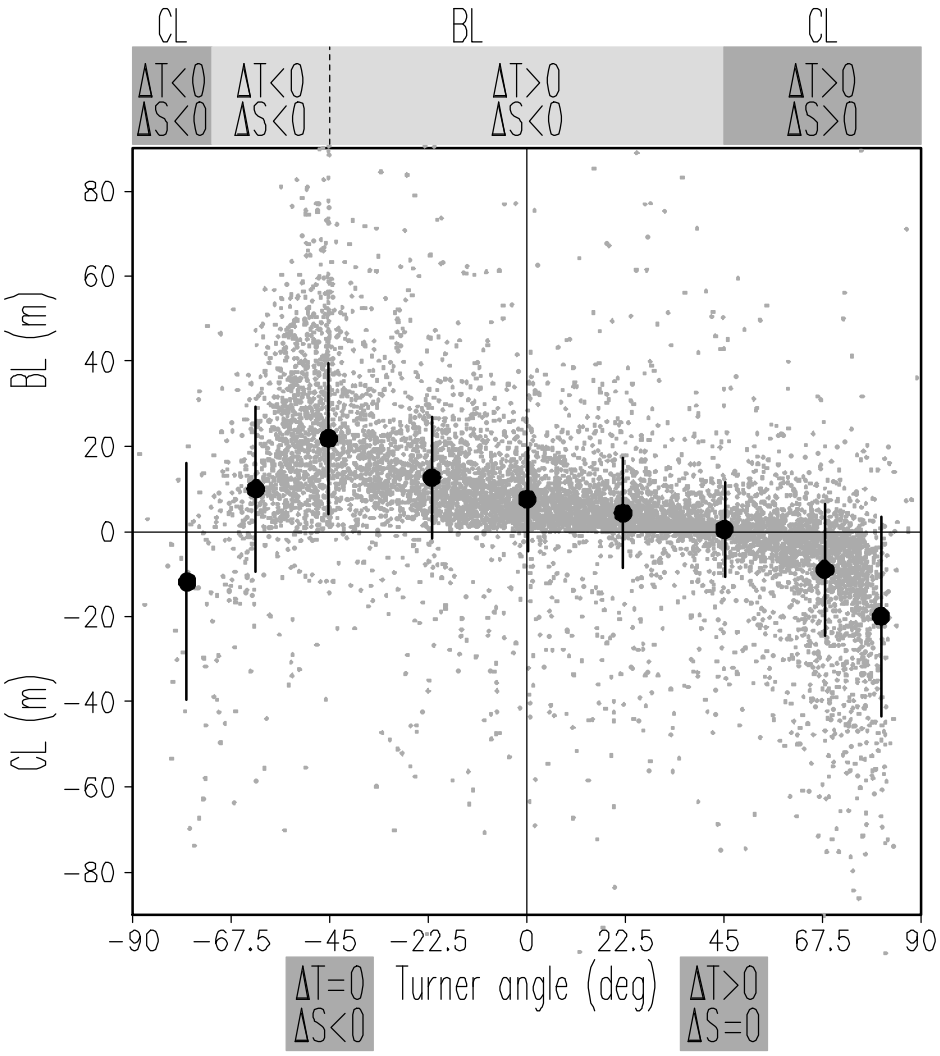


Figure 1. Observed climatological winter-spring barrier layer/compensated layer width versus bulk Turner angle evaluated using temperature ( $\Delta T$ ) and salinity ( $\Delta S$ ) difference between the top and bottom of a barrier or compensated layer. Vertical bars show the mean and the standard deviation for consecutive $22.5^0$ intervals. Grey dots show January-March data from the Northern Hemisphere and July-September data from the Southern Hemisphere. The Turner angle range $-72^0$ to $45^0$ corresponds to barrier layer. Compensated layer occurs outside this interval.

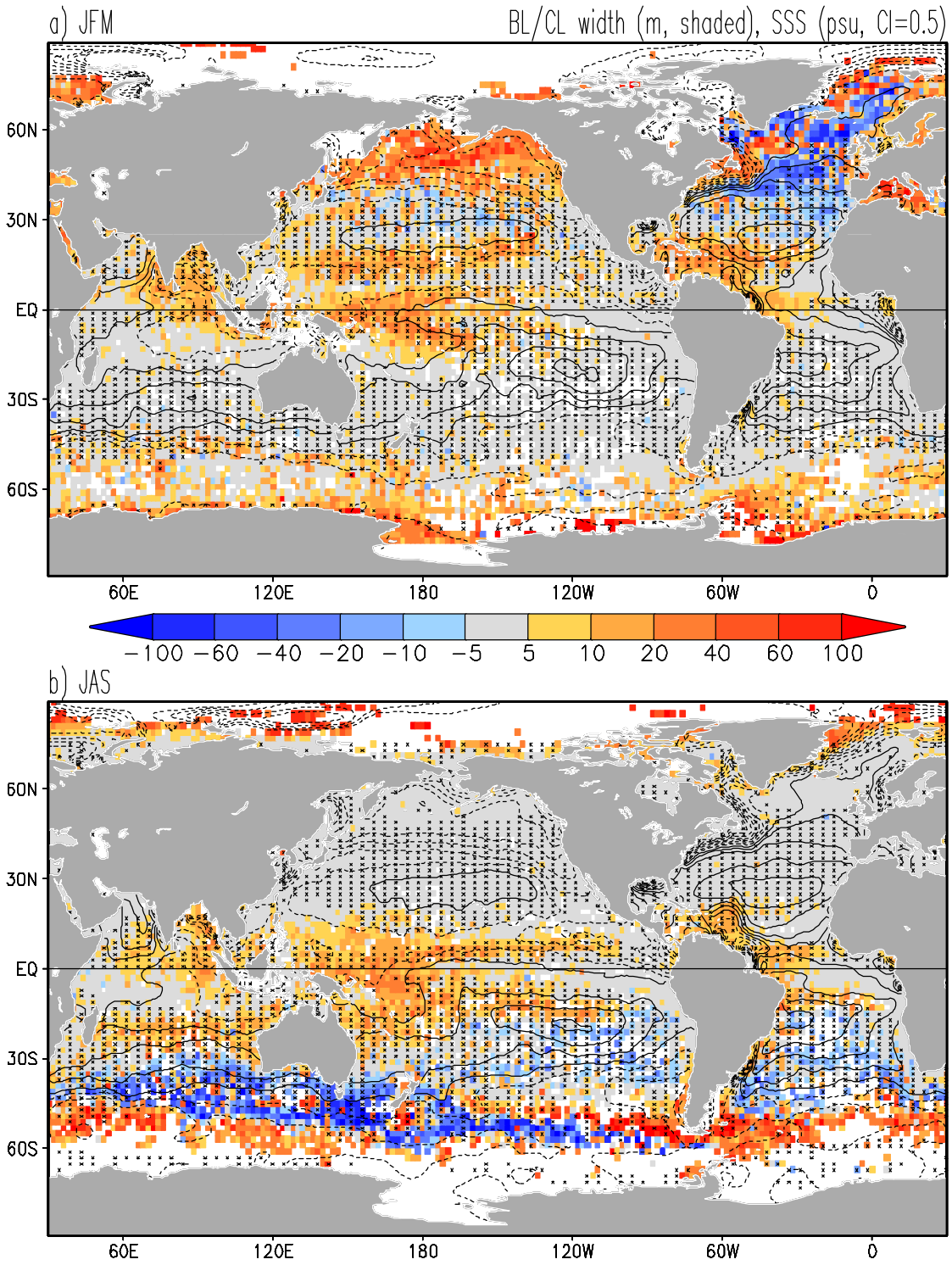


Figure 2. Observed climatological (a) January-March and (b) July-September barrier layer width (positive) and compensated layer width (negative). Climatological SSS (*Boyer et al.,* 2006, contours), SSS ≥ 35 psu (solid), SSS<35 psu (dashed). Areas of downward Ekman pumping are cross-hatched. Ekman pumping is evaluated from the QuikSCAT scatterometer winds of *Liu* (2002).

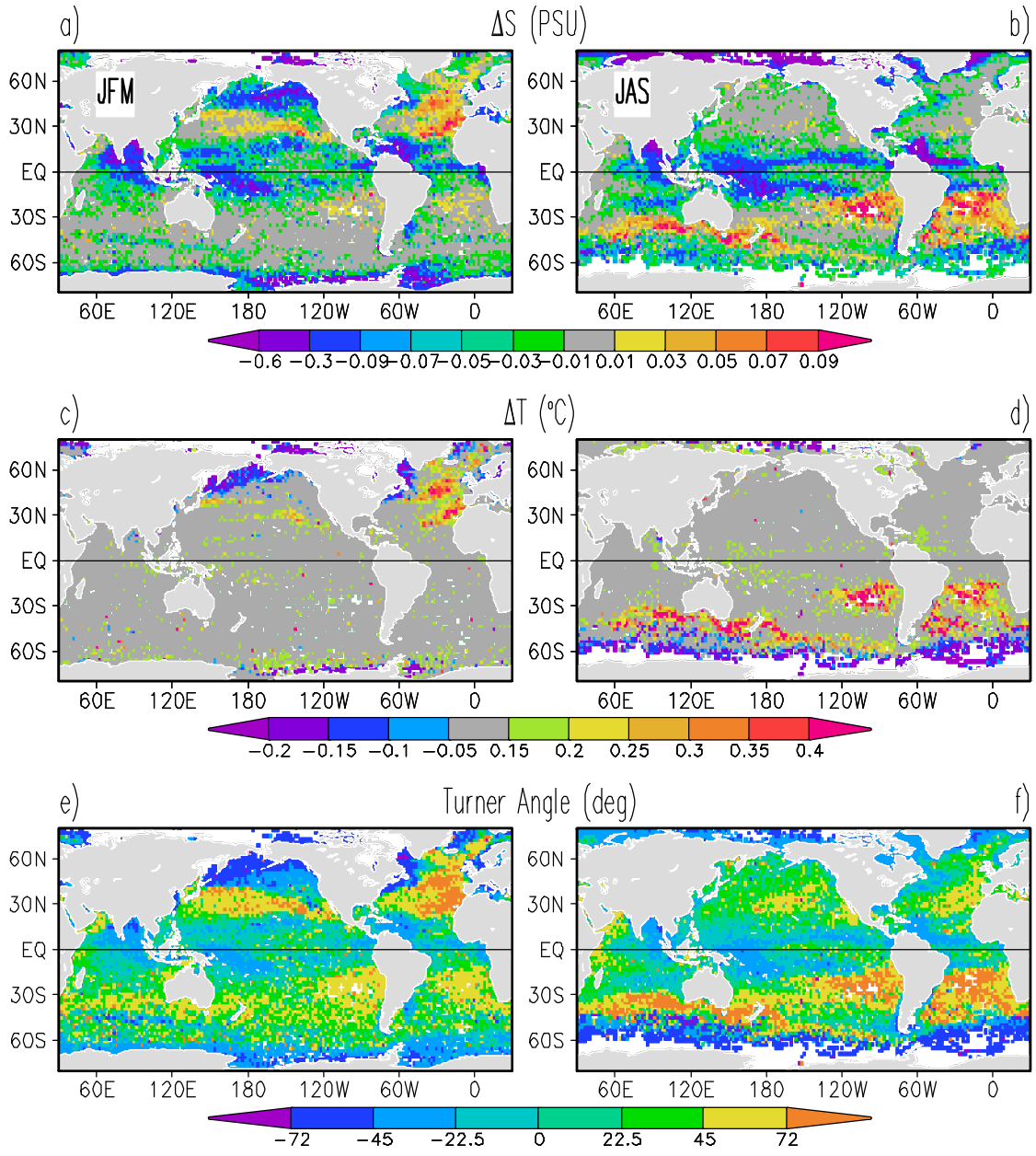


Figure 3. Observed (a,b) salinity ( $\Delta S$ ) and (c,d) temperature ( $\Delta T$ ) difference between the top $z_t$ = min[MLT, MLD] and bottom $z_b$ =max[MLT, MLD] of barrier/compensated layer, (e,f) bulk Turner angle calculated from $\Delta S$ and $\Delta T$ between the same two depths. (left) January - March (JFM) values, (right) July - September (JAS) values. Turner angles in the range from -72° to 45° correspond to barrier layers, while compensated layers occur outside this range.

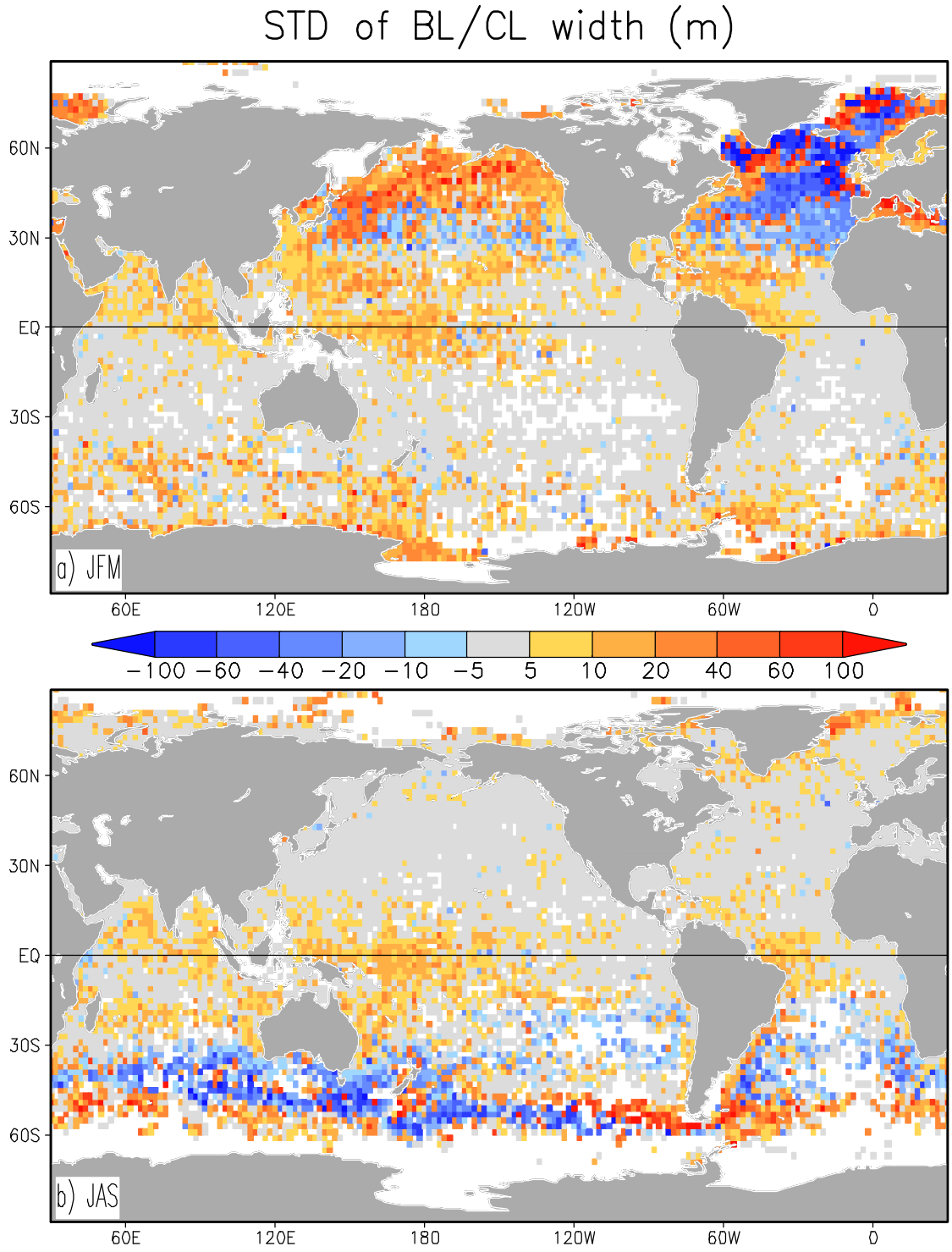


Figure 4. Standard deviation (STD) of observed (a) January-March (JFM) and (b) July-September (JAS) averaged BL/CL width. To contrast variability of barrier layer and compensated layer width, STD deviation is multiplied by the sign of corresponding 3-month average climatological BL/CL width. So the STD of barrier layer/compensated layer width is positive/negative, respectively. All values are computed from 1960-2007 data.

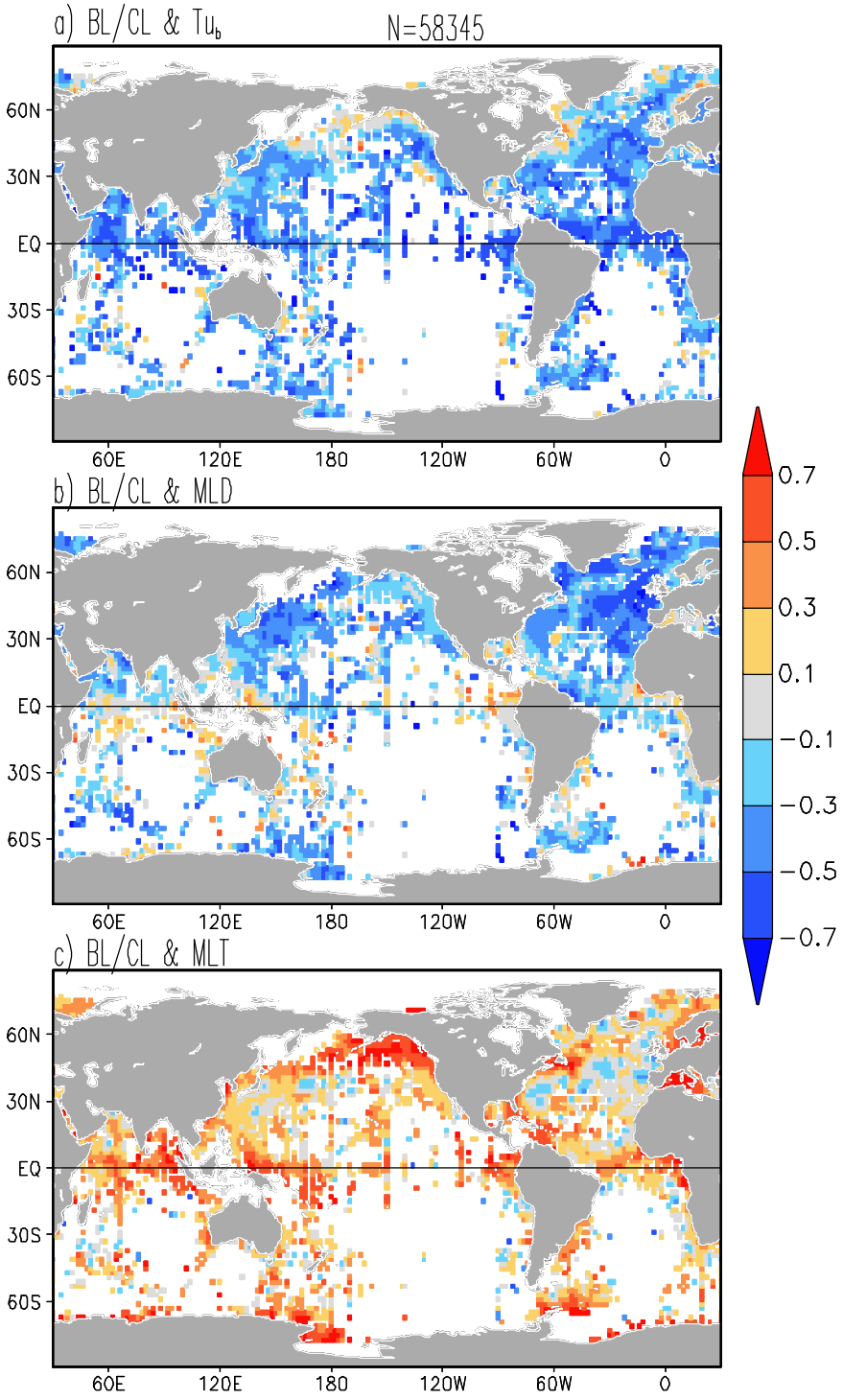


Figure 5. Time correlation of January-March average (a) BL/CL width and bulk Turner Angle, (b) BL/CL and density based mixed layer depth, (c) BL/CL and temperature based mixed layer depth. N is the total number of JFM average binned observations during 1960-2007. Correlations are shown only at grid points where at least 6 observations are available. Time correlation at every grid point is not significant, only large scale patterns matter.

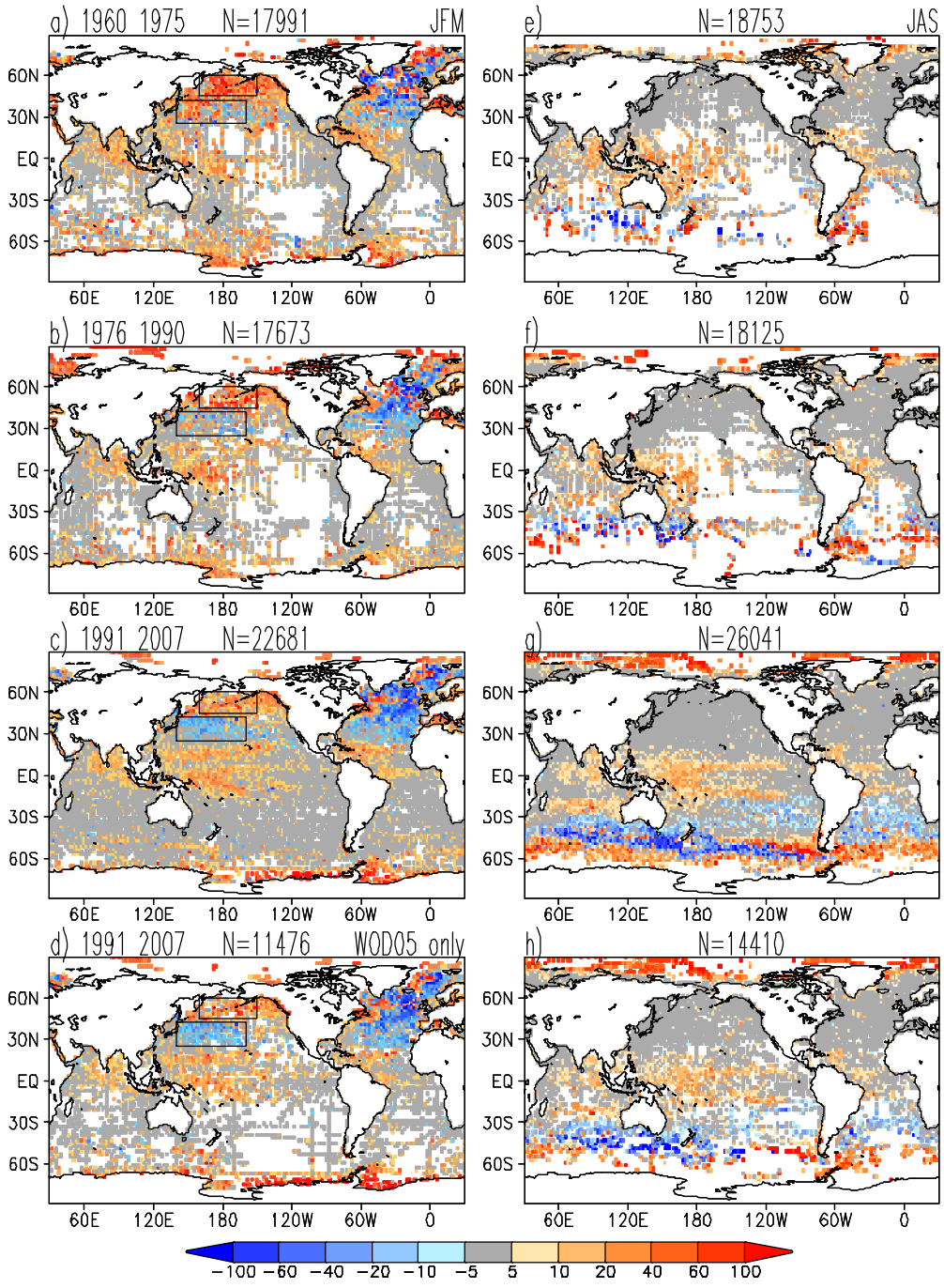


Figure 6. Quasi-decadal average barrier layer (positive) and compensated layer (negative) width in (left) northern winter and (right) austral winter. Units are meters. Rectangles show locations of the North Pacific barrier layer box (NP/BL 160°E-150°W, 45°-60°N), and the North Pacific compensated layer box (NP/CL 140°E-160°W, 25°-42°N). Bottom row shows 1991-2007 averages based on the WOD05 data, that doesn't include most of recent Argo data. *N* is the number of 3-month average observations accumulated during each 15 year period over the global ocean. There are a total of 11,000 ocean grid points on a 2°x2° grid.

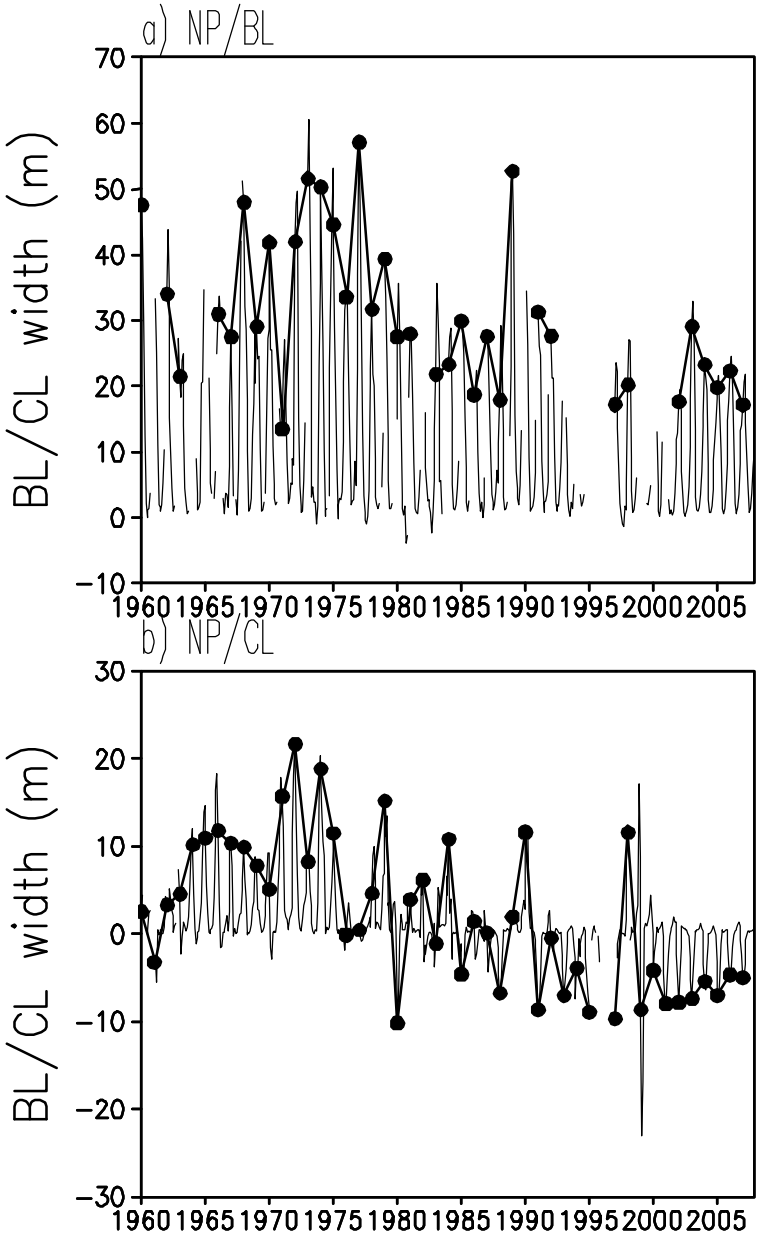


Figure 7. Box averaged BL/CL width in the (a) North Pacific barrier layer region, (b) North Pacific compensated layer region. Thin lines are 3-month running mean, bold lines are January-March averages. Data are shown if at least 10 measurements are available for box averaging. See Fig.6 for box locations.

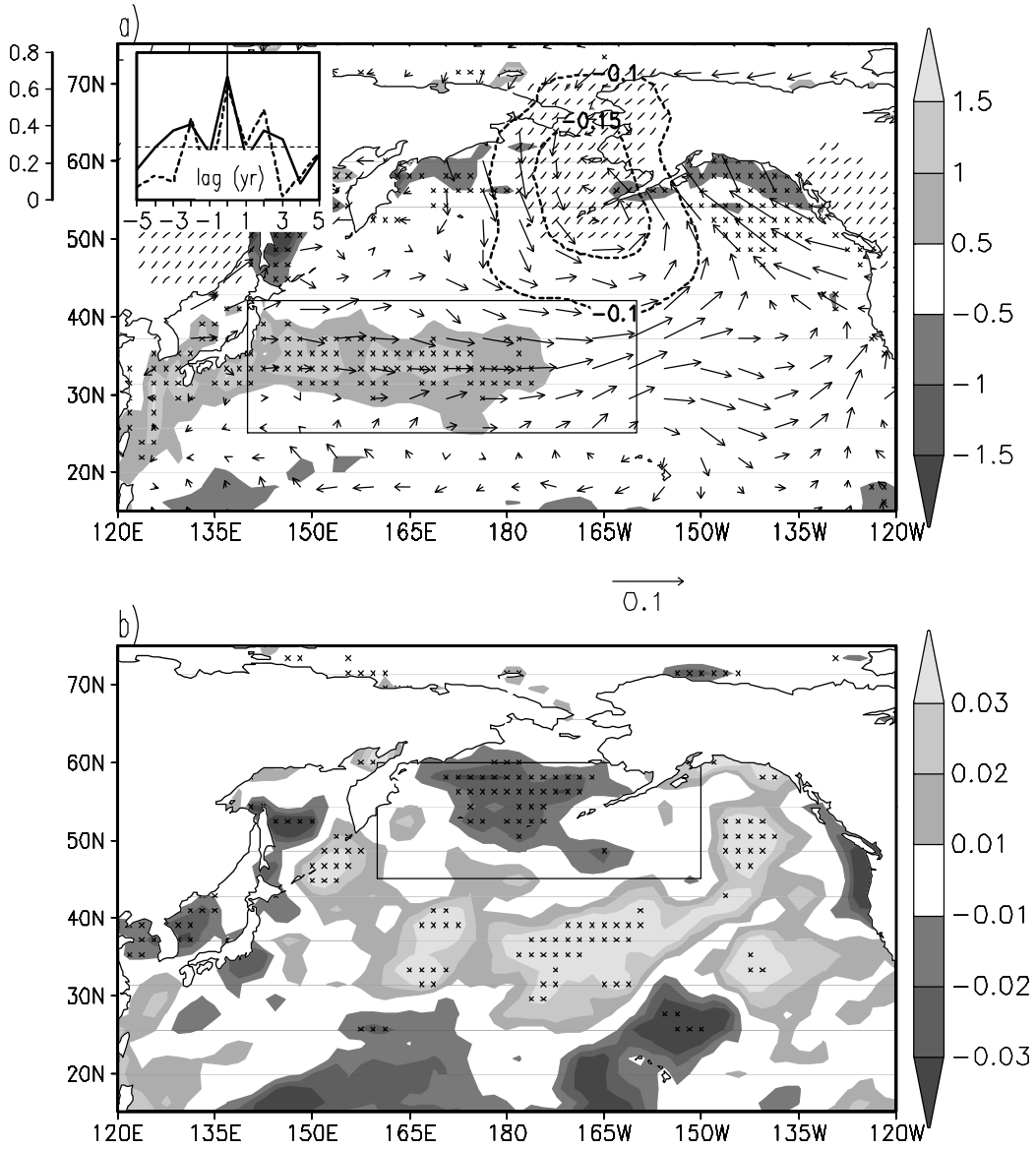


Figure 8. Linear time regression of observed 1960-2007 anomalous JFM BL/CL width in the North Pacific compensated layer box (see panel a) on anomalous (a) latent heat flux ($Wm^{-2}$/m, shading), 10m winds ($ms^{-1}$/m, arrows), mean sea level pressure (mbar/m, contours) and (b) surface precipitation rate (mm $h^{-1}$/m) elsewhere. BL/CL width time series is inverted, so that regressions correspond to widening of CLs and shrinking of BLs. Areas where time correlation with latent heat flux and precipitation is significant at the 95% level are 'X'-hatched while similar areas for air pressure are '/'-hatched. Inlay shows lagged correlation of anomalous inverted BL/CL width and MLD averaged over (solid) the NP/CL box and (dashed) the NP/BL box. The two box locations are shown in a) and b), respectively. Dashed line is the 95% confidence level of zero correlation. Positive correlation at zero lag implies that CL thickens and BL thins when the mixed layer deepens. Atmospheric parameters are provided by the NCEP/NCAR reanalysis of *Kalnay et al.* (1996).

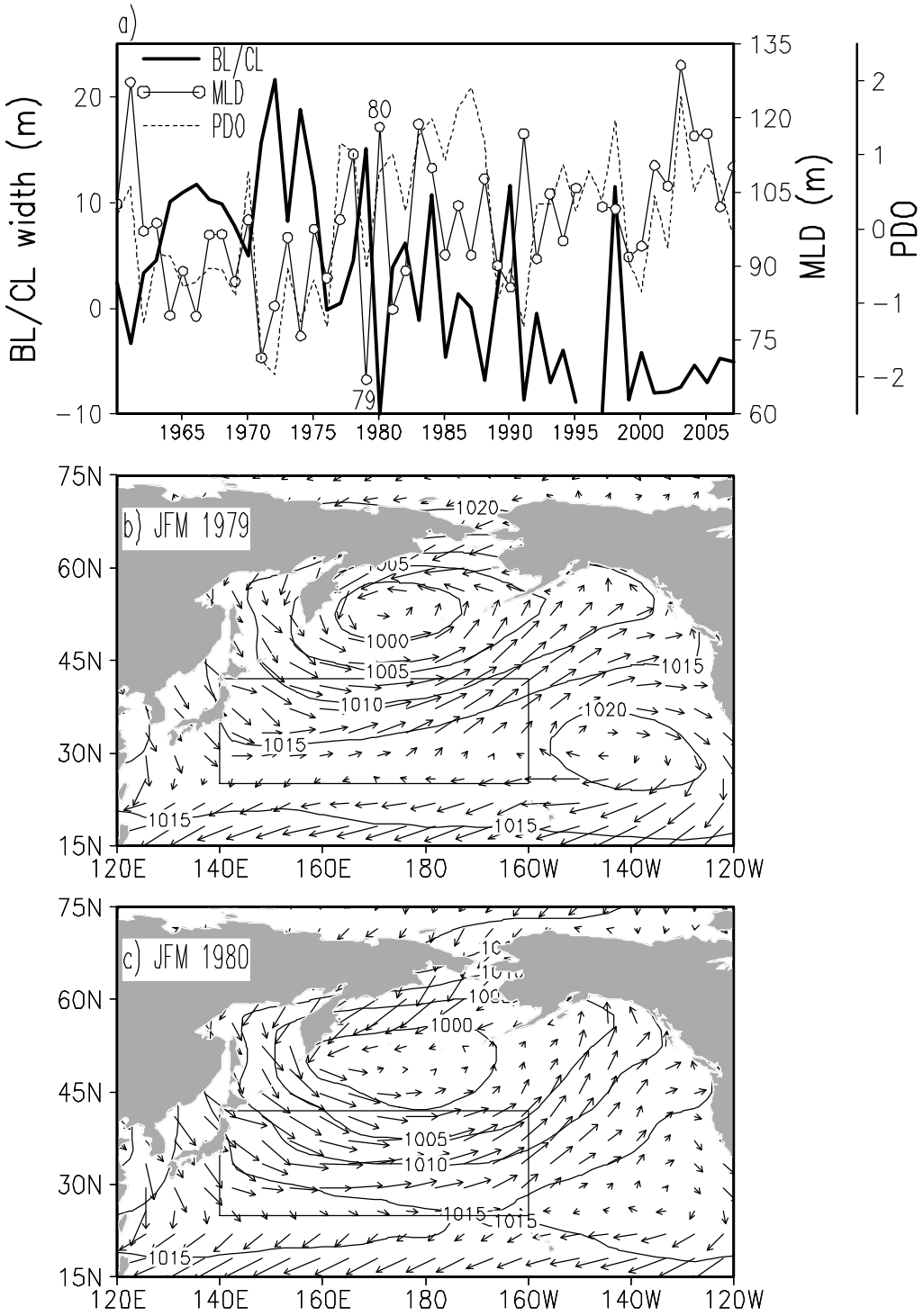


Figure 9. (a) Times series of JFM BL/CL width and MLD averaged over the NP/CL box, and the PDO index. Data is shown for years with at least 10 measurements available for box averaging. JFM winds and mean sea level pressure (mbar) for years of (b) thin and (c) thick compensated layer. Atmospheric parameters are provided by the NCEP/NCAR reanalysis of *Kalnay et al.* (1996).

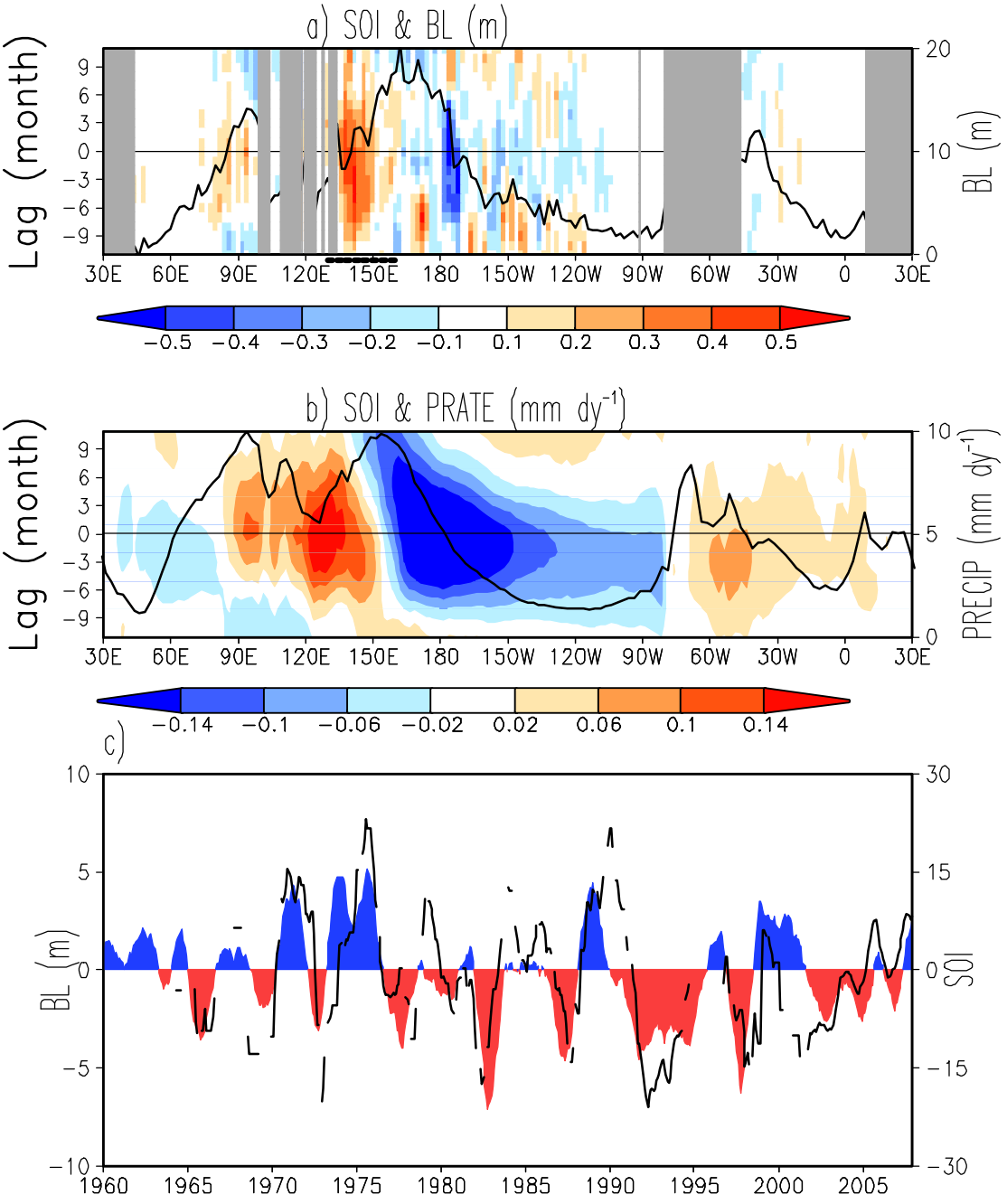


Figure 10. Lag regression of SOI on 5°S-5°N averaged (a) anomalous barrier layer width, (b) precipitation (*Xie and Arkin,* 1997). Lag regressions show magnitude in response to 1 unit change of SOI. Solid lines in (a) and (b) are time mean BL width and precipitation. Longitude bands corresponding to land are shaded gray in (a). (c) Time series of annual running mean SOI (shaded) and anomalous BL width averaged over 130°E-160°E, 5°S-5°N. Data are shown if more than 10 measurements are available for area averaging.